Elastodynamical mechanism of rate-dependent friction

Dmitri Pisarenko

Ecole Normale Supérieure, Laboratoire de géologie, 24, *rue Lhomond,* 75005 *Paris, France*

SUMMARY

We propose a model for the elastodynamical component of frictional interaction between two rough surfaces in contact. We consider the antiplane geometry and obtain the exact solution for stress within the contact of two asperities as a function of time, which includes elastic waves. The dynamical reaction of the elastic medium surrounding the asperity combined with a limited strength of the contact (characterized in the model by a modified Irwin's criterion), result in a velocity weakening friction. The origin of velocity weakening is explained by the form of the stress in the asperity as a function of time. The friction law is not imposed in the model but is obtained as the ensemble average of the frictional stress over a population of asperities. Numerical evaluation of such effective friction laws over four decades of variation of the slip velocity V leads to a $1/V$-type velocity weakening friction.

Key words: fault models, fracture, friction, velocity weakening.

INTRODUCTION

The frictional force is a product of a number of various physical phenomena that take place at the interface of sliding surfaces (Kragelsky 1965). However, in the first approximation it is possible to describe friction in terms of a simple relationship between the normal stress σ and the shear stress τ: $\tau = \mu\sigma$, where μ is the coefficient of friction. Friction is known to depend on the state of surfaces (their roughness, material properties, presence of a lubricant, etc.), as well as on the conditions of the experiment, in particular on the slip velocity. A more realistic description should therefore include a dependency of friction on the velocity $\mu(V)$, which is usually termed the friction law. The simplest example is the classical Coulomb's friction law, in which the coefficient μ takes only two values: one for zero velocity (static friction μ_s) and another for all non-zero velocities (kinematic friction μ_k, which is always smaller than μ_s). In the case of non-stationary sliding, more sophisticated empirical friction laws were suggested, which take into account the previous evolution of slip and introduce the 'memory effect' by means of so-called state variables (Dieterich 1978; Ruina 1983).

The velocity dependence of friction is of particular interest, since the decrease of the frictional resistance with the slip rate, called *velocity weakening*, is one of the parameters controlling the stability of sliding (Ruina 1983). Under certain conditions, in particular when the loading stiffness is small enough, velocity weakening friction may result in unstable stick–slip motion, which is often referred to as the physical analogue of the recurrence of earthquakes on a seismic fault (Dieterich 1972). The origin of the velocity weakening friction is still not fully understood, and a number of models were suggested that attribute it to different physical mechanisms (Dieterich 1979).

One of the possible explanations of velocity weakening is based on so-called contact strengthening. This effect consists in increasing shear resistance of the contact between the rough surfaces with duration of the static contact. It was observed for a variety of materials such as steel (Kragelsky 1965), granite (Dieterich 1972), PMMA (Berthoud & Baumberger 1998) and for contact durations ranging form 1 s to dozens of hours, that static friction was increasing with time approximately as log *t*. If we assume now that the same kind of strengthening occurs during the lifetime of an individual contact while the surfaces are sliding, this effect can lead to a velocity weakening friction. This can be illustrated in the following way: the lifetime of a contact t_c is inversely proportional to the slip velocity $t_c = d/V$, where d is some characteristic distance d (of the order of the size of an asperity). Hence the higher the slip velocity V, the shorter the average lifetime of contacts, and consequently the smaller the average contact resistance that contributes to the friction. The basic underlying physical mechanism of this ageing effect is the inelastic flow in the tips of asperities, which leads both to increasing the contact area and to formation of new contacts (Kragelsky 1965). This implies that the contribution of this mechanism to velocity weakening may be important only at low slip velocities: an 'order-of-magnitude' estimation taking $d = 10$ μm (a typical value for rough surfaces used in friction tests) and $t_c = 1$ s [for shorter contact durations no significant strengthening was observed in an ageing test with Westerly granite (Dieterich 1972)] gives $V = 10$ μm s^{-1}. This value is within the range of typical velocities of laboratory friction tests (Kilgore *et al.* 1993); however, it is orders of magnitude below the slip velocities that can occur in a fault during seismic rupture (Heaton 1990). Thus the contact ageing mechanism of velocity weakening may play its destabilizing role during the

nucleation of the seismic rupture, but not during its dynamical propagation.

Few experimental data are available on friction of rock at relatively high slip velocities, which is mainly caused by technical limitations on such laboratory measurements. Thus the friction laws used in both discrete (Burridge & Knopoff 1967; Carlson & Langer 1989) and continuous (Rice 1993; Cochard & Madariaga 1996) models of seismic faults are 'extrapolated' to high slip velocities, implicitly assuming that they show the same kind of velocity weakening behaviour as that observed experimentally at low velocities. Another important difference between the friction laws obtained from laboratory experiments and those used in models of seismic faults, are the dimensions of the corresponding physical system. In the former case the size of samples is typically a few centimetres, whereas in the latter case a fault may be as long as dozens of kilometres. Thus another important assumption of dynamical models of seismic faults is that such a scale transformation preserves the form of velocity weakening friction laws. The problem of correct re-scaling of friction laws measured in laboratory tests to the slip velocities of earthquake rupture and to the scales of seismic faults, remains essentially unresolved.

In this paper we propose to follow the approach that consists in relating microscale behaviour of elementary contacts between rough surfaces to their macroscopic characteristics, in particular to the friction law, by means of an ensemble average. The constitutive relation for the frictional interface obtained through this procedure is not based on any *a priori* hypothesis on the form of the friction law and can be re-scaled taking into account the distribution functions of microscopic parameters of the model.

We propose a model that describes the dynamical frictional interaction of two rough surfaces. It is highly simplified in that the only physical mechanisms that are taken into account are the dynamical reaction of the elastic medium surrounding an asperity, and the limited strength of the contact between two asperities. We consider the antiplane geometry and obtain an explicit solution for stress on asperity as a function of time. The model predicts a velocity weakening friction law, the origin of which can be explained by the form of the stress in the asperity as a function of time.

THE MODEL

We set the problem in the antiplane geometry (Fig. 1), which means that all the tractions are directed along the y axis and are constant along this direction. The unique displacement component u_y defines the two non-zero components of the stress tensor

$$\tau_{yx} = \partial u_y / \partial x, \quad \tau_{yz} = \partial u_y / \partial z, \tag{1}$$

thus allowing us to consider only shear waves in this geometry.

Consider two elastic half-spaces with rough surfaces separated by an interface zone within which contacts between asperities may form during a relative motion of the half-spaces in the y direction. A contact of two asperities is assumed to fix together two adjacent parts of the interface (interval $[x_1, x_2]$ in Fig. 1), and thus transmit tractions between the two surfaces. This is the central assumption of the model that simplifies the boundary conditions and reduces the problem to that of the dynamical loading of a plane interface, while the rough topography is
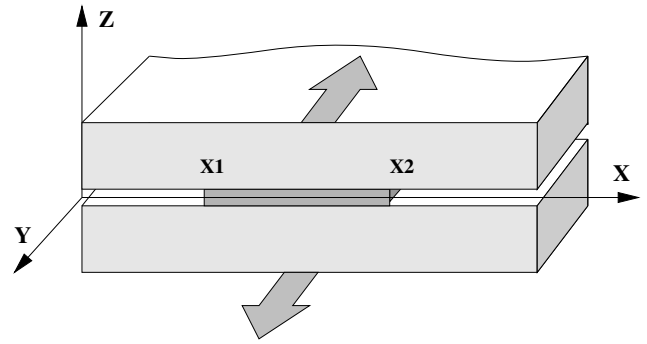

Figure 1. The antiplane geometry of the model. The interval $[x_1, x_2]$ mimics the asperity, which fixes together the adjacent parts of the two elastic half-spaces.

assumed to determine the locations of contacts and their strength. The validity of this assumption depends on the properties of the topography: such representation of the contact of rough surfaces is reasonable if their topography can be approximated by small perturbations with respect to the reference plane.

Dynamical loading of a single asperity

In this section we consider the problem of dynamical loading of a single asperity owing to the relative motion of the half-spaces. Consider two half-spaces moving at a constant speed V relative to one another in the antiplane direction, as shown in Fig. 1. At time $t = 0$, parts of the free surfaces of the half-spaces within the interval $x_1 \leq x \leq x_2$ are fixed together (this interval is referred to as contact hereafter), while outside this interval the surfaces remain free. This configuration is assumed to represent in the model the formation of a contact caused by the collision of two asperities. In the mobile reference in which both half-spaces move with the same absolute velocity $V/2$ in opposite directions, the fixed part of the interface remains at rest owing to the symmetry of the problem with respect to the plane $z = 0$. Therefore, in the initial reference associated with the lower half-space, the boundary condition is equivalent to a traction with the constant rate of displacement $V/2$ applied inside the asperity. Thus the following boundary conditions are applied to the lower half-space at $z = 0$:

$$\begin{cases} \Delta \dot{u}_y = V/2 & x_1 \leq x \leq x_2 \\ T_y = \tau_{yz} n_z = 0 & x < x_1 \quad \text{and} \quad x > x_2, \end{cases} \tag{2}$$

where T_y is the surface traction in the y direction and n_z is the normal to the interface (hereafter we shall omit coordinate subscripts and use the notation $u = u_y$, $T = T_y$ and $\tau = \tau_{yz}$).

At time $t = 0$ when the contact between the asperities is formed, the problem can be seen in an alternate way as that of an infinite elastic medium containing two semi-infinite antiplane cracks at $z = 0$, as shown in Fig. 2. The boundary conditions $\Delta \dot{u} = $ constant inside the asperity and $T = 0$ outside, do not correspond to those usually considered for crack problems, namely the traction T prescribed on crack, and zero displacement discontinuity $\Delta u = 0$ in the intact medium. However, we can construct the dynamic solution for stress inside the asperity as a combination of solutions of the two following crack problems. First consider an instantaneous laterally uniform
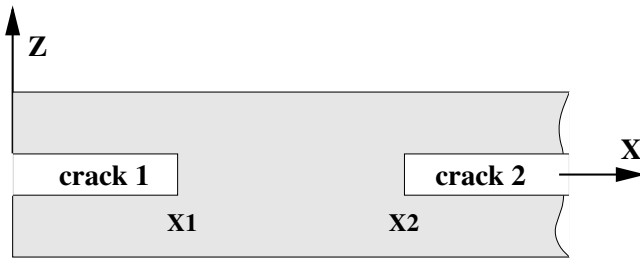
Figure 2. An equivalent representation of the asperity as two semi-infinite cracks in the elastic material extending over $[-\infty, x_1]$ and $[x_2, \infty]$.

dislocation on the surface of a half-space

$$\Delta \dot{u} = VH(t), \quad -\infty < x < \infty, \quad (3)$$

where $H(\dot{s})$ is the Heaviside function and V is the dislocation velocity. Such dislocation produces the traction on $z = 0$

$$T(t) = -\frac{\mu}{2\beta} \Delta \dot{u} = -ZVH(t), \quad -\infty < x < \infty, \quad (4)$$

where $Z = \mu/2\beta$ is the elastic impedance of the medium and β is the shear wave velocity. In the following we set $Z = 1$ without loss of generality for our purposes.

The second problem used in our construction is that of two semi-infinite cracks instantly loaded with constant tractions:

$$\begin{cases} T = VH(t) & x < x_1 \quad \text{and} \quad x > x_2 \\ \Delta \dot{u} = 0 & x_1 \leq x \leq x_2 . \end{cases} \quad (5)$$

If we now superpose the boundary conditions of these two problems, we see that outside the asperity the tractions are cancelled (free surface condition), and that the asperity is loaded by a dislocation with constant rate of displacement. Thus we find the boundary conditions of our initial problem in which the stress in the asperity is due to: (i) the instantaneous dislocation $\Delta \dot{u} = VH(t)$ and (ii) the wavefield created by discontinuities of traction at the edges of the asperity.

Let us now obtain the solution of the problem (5). It can be obtained as a superposition of solutions for two antiplane cracks and for the uniform dislocation. The stress produced by one semi-infinite crack occupying the interval $(-\infty, x_1)$ is given by the following integral (Kostrov 1966):

$$\tau_L(x, t) = \frac{1}{\pi\sqrt{x - x_1}} \int_{x-t}^{x_1} T_L(\xi, t - x + \xi) \frac{\sqrt{x_1 - \xi}}{x - \xi} d\xi, \quad x > x_1. \quad (6)$$

Similarly, for the crack extending over (x_2, ∞),

$$\tau_R(x, t) = \frac{1}{\pi\sqrt{x_2 - x}} \int_{x+t}^{x_2} T_R(\xi, t + x - \xi) \frac{\sqrt{\xi - x_2}}{x - \xi} d\xi, \quad x < x_2, \quad (7)$$

where $T(x, t)$ is the distribution of traction on crack for $t \geq 0$, and subscripts L and R refer to the left and to the right crack, respectively. We introduce the following notation:

$$\tau_L(x, t) = \frac{K_L}{\pi\sqrt{x - x_1}}, \quad \tau_R(x, t) = \frac{K_R}{\pi\sqrt{x_2 - x}}, \quad (8)$$

and calculate the integrals K_L and K_R with

$$T_L(x, t) = VH(t)H(x_1 - x),$$

and

$$T_R(x, t) = VH(t)H(x - x_2). \quad (9)$$

The result is (see the Appendix for details of the calculation)

$$K_L(t, x) = 2VH(t - x + x_1)\left(\sqrt{t + x_1 - x}\right.$$
$$\left. - \sqrt{x - x_1} \arctan \sqrt{\frac{t + x_1 - x}{x - x_1}}\right), \quad x > x_1, \quad (10)$$

and

$$K_R(t, x) = 2VH(t + x - x_2)\left(\sqrt{t + x - x_2}\right.$$
$$\left. - \sqrt{x_2 - x} \arctan \sqrt{\frac{t + x - x_2}{x_2 - x}}\right), \quad x < x_2. \quad (11)$$

The solution for stress obtained by simple superposition

$$\tau(x, t) = H(x - x_1)H(x_2 - x)[\tau_L(x, t)H(t - x + x_1)$$
$$+ \tau_R(x, t)H(t + x - x_2)] \quad (12)$$

does not take into account the reflections of waves at the asperity boundaries, and hence is only valid in the region of the space–time plane shown in grey in Fig. 3. Thus, the complete solution for the dynamical stress in an asperity instantly loaded with a constant rate displacement V is

$$\tau(x, t) = V\left[\frac{1}{2} + \frac{H(t - x + x_1)}{\pi\sqrt{x - x_1}}\left(\sqrt{t + x_1 - x}\right.\right.$$
$$\left. - \sqrt{x - x_1} \arctan \sqrt{\frac{t + x_1 - x}{x - x_1}}\right)$$
$$+ \frac{H(t + x - x_2)}{\pi\sqrt{x_2 - x}}\left(\sqrt{t + x - x_2}\right.$$
$$\left.\left. - \sqrt{x_2 - x} \arctan \sqrt{\frac{t + x - x_2}{x_2 - x}}\right)\right], \quad x_1 < x < x_2,$$
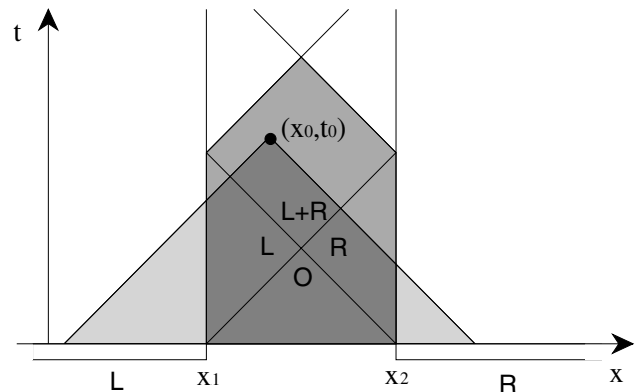
$$(13)$$

Figure 3. Space–time domain of calculation of the stress in the asperity at a given observation point (x_0, t_0). The contributions to the dynamical stress field from the left (L) and right (R) edges of the asperity propagate with the speed of elastic waves. The grey region delimits the domain of validity of eq. (13).

assuming that the observation point (x_0, t_0) is located within the grey region in Fig. 3. The stress field given by this solution as a function of time and of space coordinate is shown in Fig. 4. It shows an instantaneous jump at $t = 0$ due to the 'collision' of asperities (dislocation effect) and $1/\sqrt{x}$-type singularities (stress concentrations) at the edges of the asperity, in accordance with the ideally elastic continuous medium theory.

By taking the integral of stress $\tau(x, t)$ over x at a fixed time t we obtain the force exerted by the asperity

$$F(t) = \int_{x_1}^{x_2} \tau(x, t) \, dx, \tag{14}$$

which can be seen as the instantaneous contribution of the asperity to friction.

In order to complete the formulation of our friction model we shall now set the fracture criterion and calculate the *average* frictional resistance of a single asperity.

Fracture criterion

The conditions under which fracture occurs in brittle elastic solids are generally described in terms of a specific fracture criterion. The most widely accepted are Griffith's and Irwin's criteria (Freund 1989). Griffith's criterion is based on the energy balance of a crack, and hence characterizes the state of the crack globally, which makes it not quite convenient for our model. According to Irwin's criterion, rupture occurs if the stress intensity factor K, which represents the 'weight' of the singularity of the stress field, exceeds some critical value K_{cr}. We can readily apply this fracture criterion to our problem, since the integrals K_L and K_R calculated above are in fact the stress intensity factors for the left- and for the right-hand edges of the asperity, respectively. However, Irwin's criterion takes into account only the singular stress component produced by the discontinuity of the boundary condition. Hence all non-singular terms of the full stress field eq. (13), including the wave emanating from the opposite edge of the asperity, are neglected. This is an important shortcoming since physically the whole stress field contributes to the nucleation of the fracture.

The singularity of the stress field on the asperity edge arises from the discontinuity of the boundary condition treated within the continuous medium formalism. An idealized continuous elastic solid has no internal scale, and therefore such a boundary condition results in a singular stress concentration. In reality this singularity is 'regularized' (smoothed) at the smallest scale of natural discontinuities of the medium (e.g. at the scale of microcrystals or rock grains), which means that below this scale the continuous stress field is not well defined and one should rather operate with forces on the boundaries of discontinuities. This small-scale cut-off is physically equivalent to averaging of the stress field over some characteristic distance d:

$$\tau_d(x, t) = \frac{1}{d} \int_{x-d/2}^{x+d/2} \tau(x', t) \, dx'. \tag{15}$$

The resulting integrated stress field τ_d is free of singularities and at the same time includes contributions from all stress terms. We can then compare the averaged stress with a critical threshold value and use it as a new local fracture criterion, which takes into account all stress components. Note that in our model, the fracture threshold is a characteristic of a *contact* of two asperities and not that of the material itself, thus it may depend on other parameters, such as normal load, asperity height, etc.

Since the $1/\sqrt{x}$-type singularities are integrable, we can obtain the expression for the smoothed stress τ_d at the asperity edge by integrating eq. (13) over the heterogeneity scale parameter d (this is done in the Appendix). Fig. 5 shows the integrated stress τ_d at the asperity edge as a function of time. The solid line shows the full stress field, including the arrival of wave from the opposite edge of the asperity (clearly visible at $t = 2$), while the dashed line gives the stress due only to the left-hand edge, similar to the stress intensity factor criterion.

EFFECTIVE FRICTION LAWS

We assume that in our model an asperity represents the 'elementary scale' of the interface between the rough surfaces, and consequently its behaviour cannot be described in terms of a friction law. Therefore, we need to establish the relationship between the dynamical contribution to friction of a single
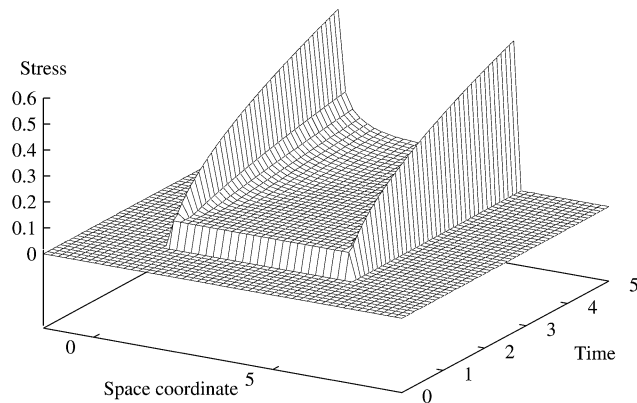
Figure 4. Evolution of the dynamical stress field in the asperity extending over [0, 5] calculated according to eq. (13). The stress is singular at the edges of the asperity and was truncated for the purpose of the graphical representation by shifting the graph mesh with respect to the asperity edges. Note the instantaneous jump of the stress at $t = 1$ when the asperity is abruptly loaded at constant displacement rate.
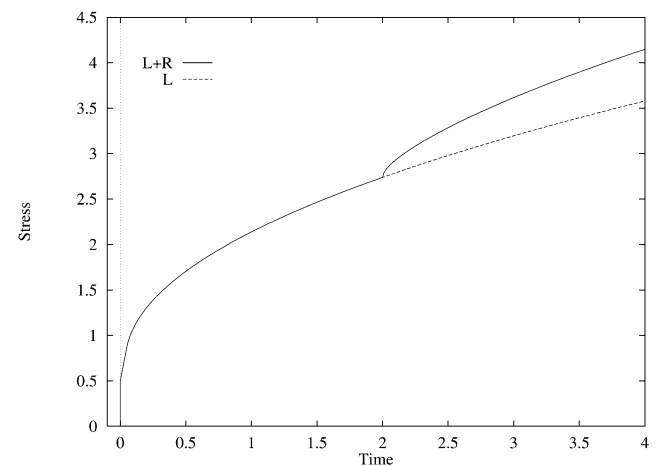
Figure 5. Integrated stress τ_d at the asperity edge as a function of time calculated according to eq. (15). The dashed line shows the stress taking into account only one edge of the asperity, the solid line corresponds to the full solution where the elastic wave emanating from the other edge of the asperity (arriving at $t = 2$) is also taken into account.

asperity at a microscopic scale, on one hand, and a friction law for the contact between rough surfaces containing a large number of such asperities on the other hand. This can be achieved by assuming some form of distribution of the physical parameters of contacts between asperities, and by performing an ensemble average over the population of contacts (which implies the assumption of homogeneity of those distributions over the whole surface). This is quite similar to the approach taken in the molecular kinetic theory of gases, except that in our case instead of molecules we deal with contacts between asperities, which form, exist for some time and disappear due to the sliding of the rough surfaces.

The input parameters of the model can thus be directly related to the properties of the contact between the rough surfaces. The topography of the surfaces and an adequate contact model will determine an ensemble of N contacts between asperities with their locations, $x^{(i)}$, their widths $w^{(i)} = x_2^{(i)} - x_1^{(i)}$, and the corresponding rupture thresholds $\tau_{cr}^{(i)}$, $i = 1, 2, \ldots, N$.

Here we consider the simplest case of non-interacting contacts. Since we neglect the elastic interactions between the asperities in this case, their locations will determine only the occurrence of contacts in time, which will be uncorrelated in this case. Therefore, the frictional resistance of an ensemble of such contacts can be estimated through a simple time average of the force exerted by a single contact:

$$\langle F \rangle = \lim_{T \to \infty} \frac{1}{T} \int_0^T \int_{x_1}^{x_2} \tau(\xi, t') \, d\xi \, dt' . \tag{16}$$

Since each asperity undergoes a sequence of identical loading and breaking cycles, we can calculate the time average over one such cycle and normalize it using the density of contacts:

$$\langle F \rangle = \frac{1}{T} \int_0^{t_c} \int_{x_1}^{x_2} \tau(\xi, t') \, d\xi \, dt' , \tag{17}$$

where the integration over time was limited by t_c, since the asperity contributes to the frictional resistance only during the lifetime of the contact t_c. It is clear that for all sliding velocities V, the normalizing time interval T must correspond to the same *slip* L, where $1/L$ is the linear contact density. Thus we finally obtain:

$$\langle F \rangle = \frac{V}{4} \int_0^{t_c} \int_{x_1}^{x_2} \tau(\xi, t') \, d\xi \, dt' \tag{18}$$

Expression (18) allows us to calculate the dependence of the average frictional resistance of an ensemble of non-interacting asperities as a function of the slip velocity $\langle F \rangle(V)$, which henceforth we call the effective friction law. The dependence of the average frictional force on the velocity is non-linear since the contact duration t_c depends on the velocity in a non-linear manner. Two effective friction laws $\langle F \rangle(V)$ evaluated numerically according to eq. (18)) and averaged over 5×10^6 independent asperities are shown in Fig. 6. The first of them ($\diamondsuit$ signs on the graph) was calculated using an ensemble of identical contacts [$w^{(i)} = w$ and $\tau_{cr}^{(i)} = \tau_{cr}$], while the second corresponds to an ensemble of contacts with a uniform distribution of width $w^{(i)}$ (with the same mean value as in the first case and the spread equal to 50 per cent of the mean) and a Gaussian distribution of strength thresholds $\tau_{cr}^{(i)}$. Both curves
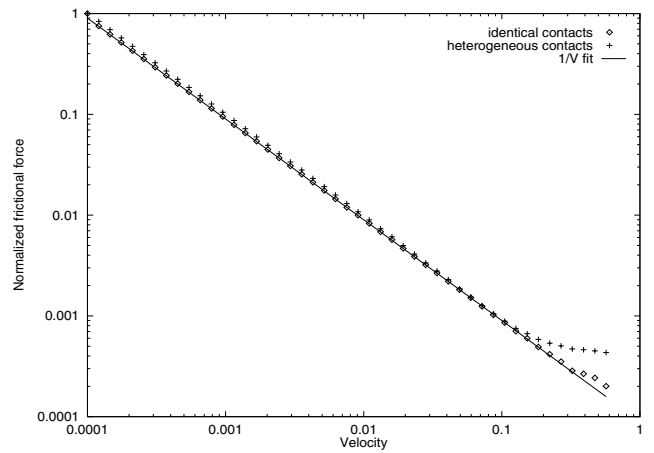
Figure 6. Effective friction laws for an ensemble of 5×10^6 independent identical ($\diamondsuit$ signs) and heterogeneous ($+$ signs) asperities with a random uniform distribution of widths and a Gaussian distribution of strengths; solid line represents a $1/V$ fit. The frictional force is normalized to its value at the minimal velocity. Note the universal $1/V$ velocity weakening friction and the relative insensitivity of the discussed friction mechanism to the particular form of distribution of the asperity parameters.

are remarkably close to a $1/V$ dependence over four decades of the slip velocity variations. A somewhat stronger scatter of the estimated values of the effective friction laws around the $1/V$ fit at the right-hand end of the graph is caused by the decreasing precision of the numerical evaluation of the time integral in eq. (18) for short contact durations t_c at high slip velocities.

The $1/V$-type friction laws were used in models of seismic faults by a number of authors in rate-dependent (Shaw *et al.* 1994) and in more general rate- and state-dependent formulations (Rice 1993). The important feature of such models is the unstable regime of slip that is provided by a sufficiently steep decrease of friction with velocity, independent of the particular form of this functional dependence. However, such velocity weakening friction laws were introduced into those models on a purely empirical basis. Indeed, no direct measurements of friction on seismic faults are available, and the extrapolation of friction laws observed in laboratory tests on rock samples to fault scales is a delicate problem. Friction tests on rock samples performed over a wide range of conditions (see, e.g., Kilgore *et al.* 1993) show a variety of behaviour, including velocity strengthening and velocity weakening, depending on the velocity range, normal load, temperature etc. Thus at least for some subset of experimental conditions, one can assume velocity weakening friction in faults on observational grounds. Unfortunately, the range of slip velocities in classical laboratory friction tests is quite limited owing to technical constraints, and typically does not exceed a few mm s^{-1}. Such slip velocities are orders of magnitude below slip velocities in a fault during an earthquake, which can be inferred from near-field seismic records (Heaton 1990). A simple extrapolation of laboratory friction laws to higher slip rates can hardly be justified, since dynamical effects should play an increasingly important role at high velocities. Therefore, the elastodynamical velocity weakening microscopic mechanism of friction and the ensemble average approach discussed in the present work may provide an alternative way of introducing friction into large-scale fault models, since they are not based on any particular *a priori* form of friction law.

CONCLUSIONS

Dynamical friction involves a complex combination of a number of different physical mechanisms that may have a strengthening (stabilizing) or weakening (destabilizing) effect and the importance of which depends on the slip velocity. We introduced a model in which we isolated one of these mechanisms, namely the dynamical breaking of asperities, and studied its contribution to friction. It was found that this mechanism leads to velocity weakening friction over a wide range of velocities, practically up to the speed of elastic waves. It is remarkable that the effective friction law predicted by this model for an ensemble of non-interacting asperities has a very simple $1/V$ form, while it derives from a quite complex evolution of stress in each asperity at the microscopic level. The form of the effective friction law was found to be not very sensitive to a particular distribution of contact widths and strengths (that can be related to the roughness of surfaces). This suggests that the studied mechanism of velocity weakening is essentially caused by the elasto-dynamical effects, since it is produced by the model even in the case of non-interacting identical asperities.

The described mechanism of velocity weakening friction can thus support certain models of seismic rupture in which a weakening factor is needed at high slip velocities, where other mechanisms based on slow inelastic processes are inefficient.

REFERENCES

Berthoud, P. & Baumberger, T., 1998. Role of asperity creep in time- and velocity-dependent friction of a polymer glass, *Europhys. Lett.,* **41,** 617–622.

Burridge, R. & Knopoff, L., 1967. Model and theoretical seismicity, *Bull. seism. Soc. Am.,* **57,** 341–371.

Carlson, J.M. & Langer, J.S., 1989. Properties of earthquakes generated by fault dynamics, *Phys. Rev. Lett.,* **62,** 2632–2635.

Cochard, A. & Madariaga, R., 1996. Complexity of seismicity due to highly rate-dependent friction, *J. geophys. Res.,* **101,** 25 321–25 336.

Dieterich, J., 1972. Time-dependent friction in rocks, *J. geophys. Res.,* **77,** 3690–3697.

Dieterich, J., 1972. Time-dependent friction as a possible mechanism for aftershocks, *J. geophys. Res.,* **77,** 3771–3781.

Dieterich, J., 1978. Time-dependent friction and the mechanics of stick slip, *Pure appl. Geophys.,* **116,** 790–806.

Dieterich, J., 1979. Modeling of rock friction 1. Experimental results and constitutive equations, *J. geophys. Res.,* **84,** 2161–2168.

Freund, L.B., 1989. *Dynamic Fracture Mechanics,* Cambridge University Press, Cambridge.

Heaton, T.H., 1990. Evidence for and implications of self-healing pulses of slip in earthquake rupture, *Phys. Earth planter. Inter.,* **64,** 1–20.

Kilgore, B.D., Blanpied, M.L. & Dieterich, J.H., 1993. Velocity dependent friction of granite over a wide range of conditions, *Geophys. Res. Lett.,* **20,** 903–906.

Kostrov, B.V., 1966. Unsteady propagation of longitudinal shear cracks, *J. Appl. Math. Mech.,* **30,** 1241–1248.

Kragelsky, I.V., 1965. *Friction and Wear,* Butterworths, WA.

Rice, J.R., 1993. Spatio-temporal complexity of slip on a fault, *J. geophys. Res.,* **98,** 9885–9907.

Ruina, A., 1983. Slip instability and state variable friction laws, *J. geophys. Res.,* **88,** 10 359–10 370.

Shaw, B.E., Carlson, J.M. & Langer, J.S., 1994. Patterns of seismic activity preceeding large earthquakes, *J. geophys. Res.,* **97,** 479–488.

APPENDIX A: EXPRESSIONS FOR THE STRESS INTEGRATED OVER THE ASPERITY WIDTH [X_1, X_2] (FRICTIONAL FORCE)

We denote

$$x_2 - x_1 = D.$$

The edge dislocation component of the stress field is then

$$F_e = \int_{x_1}^{x_2} V\, dx = VD. \tag{A1}$$

A1   First case: $t \leq D$

The contribution from the left-hand edge of the asperity ($x \geq x_1$ and $t \geq x - x_1$) yields:

$$F_L(t) = \frac{2V}{\pi} \int_{x_1}^{x_1+t} \sqrt{\frac{t + x_1 - x}{x - x_1}}\, dx$$

$$- \frac{2V}{\pi} \int_{x_1}^{x_1+t} \arctan \sqrt{\frac{t + x_1 - x}{x - x_1}}\, dx = \frac{2V}{\pi}\left(I_1 - I_2\right). \tag{A2}$$

Denoting

$$x - x_1 = R, \quad \text{and} \quad dx = dR,$$

we obtain

$$I_1 = \int_0^t \sqrt{\frac{t - R}{R}}\, dR = \frac{\pi}{2}\, t, \tag{A3}$$

and

$$I_2 = \int_0^t \arctan \sqrt{\frac{t - R}{R}}\, dR = \frac{\pi}{4}\, t. \tag{A4}$$

The contribution from the right-hand edge of the asperity ($x \leq x_2$ and $t \geq x_2 - x$) yields

$$F_R(t) = \frac{2V}{\pi} \int_{x_2-t}^{x_2} \sqrt{\frac{t + x - x_2}{x_2 - x}}\, dx$$

$$- \frac{2V}{\pi} \int_{x_2-t}^{x_2} \arctan \sqrt{\frac{t + x - x_2}{x_2 - x}}\, dx = \frac{2V}{\pi}\left(I_3 - I_4\right), \tag{A5}$$

where

$$x_2 - x = W = D - R \quad \text{and} \quad dx = -dW.$$

Then

$$I_3 = -\int_t^0 \sqrt{\frac{t - W}{W}}\, dW = \int_0^t \sqrt{\frac{t - W}{W}} = I_1, \tag{A6}$$

and

$$I_4 = \int_0^t \arctan\sqrt{\frac{t-W}{W}}\,dw = I_2\,. \tag{A7}$$

The total force produced by the asperity is then (when $t \le D$):

$$F(t) = VD + \frac{2V}{\pi}\left[(I_1 - I_2) + (I_3 - I_4)\right]$$

$$= VD + V(t/2 + t/2) = VD + Vt\,. \tag{A8}$$

A2 Second case: $t > D$

The contribution from the left-hand edge of the asperity ($x \ge x_1$ and $t \ge D$) yields

$$F_{\mathrm{L}}(t) = \frac{2V}{\pi}\int_{x_1}^{x_2}\sqrt{\frac{t+x_1-x}{x-x_1}}\,dx$$

$$- \frac{2V}{\pi}\int_{x_1}^{x_2}\arctan\sqrt{\frac{t+x_1-x}{x-x_1}}\,dx = \frac{2V}{\pi}(I_1 - I_2)\,, \tag{A9}$$

with

$$I_1 = \int_0^D \sqrt{\frac{t-R}{R}}\,dR$$

$$= \frac{\pi}{4}t + \sqrt{D(t-D)} + \frac{t}{2}\arctan\left(\frac{2D-t}{2\sqrt{D(t-D)}}\right), \tag{A10}$$

and

$$I_2 = \int_0^D \arctan\sqrt{\frac{t-R}{R}}\,dR = \frac{\pi}{8}t - \frac{1}{2}\sqrt{D(t-D)}$$

$$+ D\arctan\sqrt{\frac{t-D}{D}} - \frac{t}{4}\arctan\left(\frac{2D-t}{2\sqrt{D(t-D)}}\right). \tag{A11}$$

The contribution from the right-hand edge of the asperity ($x \le x_2$ and $t \ge D$) yields

$$F_{\mathrm{R}}(t) = \frac{2V}{\pi}\int_{x_1}^{x_2}\sqrt{\frac{t+x-x_2}{x_2-x}}\,dx - \frac{2V}{\pi}\int_{x_1}^{x_2}\arctan\sqrt{\frac{t+x-x_2}{x_2-x}}\,dx$$

$$= \frac{2V}{\pi}(I_3 - I_4)\,, \tag{A12}$$

with

$$I_3 = -\int_D^0 \sqrt{\frac{t-W}{W}}\,dW = \int_0^D \sqrt{\frac{t-W}{W}} = I_1\,, \tag{A13}$$

and

$$I_4 = \int_0^D \arctan\sqrt{\frac{t-W}{W}}\,dW = I_2\,. \tag{A14}$$

The total force on the asperity (when $t > D$) is then

$$F(t) = VD + \frac{4V}{\pi}(I_1 - I_2)$$

$$= VD + \frac{4V}{\pi}\left(\frac{\pi}{8}t + \frac{3}{2}\sqrt{D(t-D)}\right.$$

$$\left. - D\arctan\sqrt{\frac{t-D}{D}} + \frac{t}{4}\arctan\left[\frac{2D-t}{2\sqrt{D(t-D)}}\right]\right). \tag{A15}$$

APPENDIX B: EXPRESSION FOR THE STRESS AT THE EDGE OF THE ASPERITY AVERAGED OVER THE SMALL-SCALE PARAMETER

We only consider here the case $t \ge d$, since the small-scale parameter d can always be chosen smaller than the integration time-step.

$$\tau_d(x_1, t) = V\left[1 + \frac{1}{d}\int_{x_1}^{x_1+d}\tau_{\mathrm{L}}(x,t)\,dx + \tau_{\mathrm{R}}(x_1,t)\right]$$

$$= V\left[1 + \frac{2}{\pi d}\left(\int_0^d \sqrt{\frac{t-R}{R}}\,dR - \int_0^d \arctan\sqrt{\frac{t-R}{R}}\,dR\right)\right.$$

$$\left. + \frac{2}{\pi}H(t-D)\left(\sqrt{\frac{t-D}{D}} - \arctan\sqrt{\frac{t-D}{D}}\right)\right]$$

$$= V\left[1 + \frac{2}{\pi d}(I_5 - I_6)\right.$$

$$\left. + \frac{2}{\pi}H(t-D)\left(\sqrt{\frac{t-D}{D}} - \arctan\sqrt{\frac{t-D}{D}}\right)\right], \tag{B1}$$

where $H(\cdot)$ is the Heaviside function, and

$$I_5 - I_6 = \frac{\pi}{8}t + \frac{3}{2}\sqrt{d(t-d)}$$

$$- d\arctan\sqrt{\frac{t-d}{d}} + \frac{t}{4}\arctan\left[\frac{2d-t}{2\sqrt{d(t-d)}}\right]. \tag{B2}$$